ATI Advanced Technology Institute | Electrical & Electronic Engineering

High-Electric-Field Nanoscience

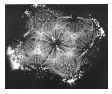

UNIVERSITY OF SURREY

PROGRESS IN RESHAPING FIELD ELECTRON EMISSION THEORY FOR THE BENEFIT OF EXPERIMENTAL SCIENTISTS AND ENGINEERS

Richard G. Forbes

Advanced Technology Institute &
Dept. of Electrical and Electronic Engineering,
University of Surrey

IVESC & ITG-IVEW 2020

[Virtual Meeting, May 2020]

NOTE

Given that this is a pdf-file presentation to a virtual meeting, without oral commentary, the best approach has seemed to be to prepare a presentation with additional written explanation, and to include references to material where further details of the author's approach can be found. References are given at the end of the presentation.

This presentation is a slightly updated version of one given at the 2019 IVESC/IVNC meeting in Cincinnatti [R1]. Apologies to those who have seen much of this material before, but I think the majority of the audience will not have done so.

In this presentation, all universal constants are given to 7 significant figures, but it is assumed that in practice these will be mathematically approximated, as suits the context.

The author's permanent e-mail alias is: r.forbes@trinity.cantab.net .

Introduction (1)

Long-term aim is to put field electron emission (FE) onto a better scientific basis.

This means

(a) Improved theoretical treatments.

(b) Better methodologies for comparing theory and experiment.

There has been much useful recent progress in developing FE theory.

But aspects of our FE experimental data analysis, especially the analysis of measured current-voltage (I_m–V_m) data, are about 90 years behind where the theory currently is.

There seems an urgent need to improve FE I_m–V_m data-interpretation methodologies, and to define and encourage "best practice".

This presentation is primarily about FE data-analysis methodologies and underlying theoretical developments.

Introduction (2)

In the longer term, this better FE science needs to be able to deal precisely, not only with relatively blunt metal emitters operating at room temperature, but also with

- **(a) non-metallic emitters, especially semi-conductors & carbon nanotubes;**
- **(b) emitters with realistic shapes, including sharply pointed and "atomically sharp" emitters.**
- **(c) emitters operating at temperatures somewhat above room temperature.**

However, current reality is that (whatever the material and the nature of the emitter) virtually all FE data analysis is carried out within a physical model that disregards the existence of atoms, uses the Sommerfeld free-electron-metal model, treats the emitter as it had a smooth planar surface, and takes the emitter temperature as effectively zero.

Current reality is that, even within the context of this simplified model, many technological papers make conceptual/procedural errors of various kinds, and some consequently publish spurious emitter characterization data.

Introduction (3)

Thus, improvement needs be a multi-stage process.

Stage 1 is to develop and implement

"21st Century smooth-planar-metal-like-emitter (SPME) methodology"

Later stages will need to involve consolidation and development of

"point-form emitter methodologies", and

"atomic-level methodologies".

This presentation is primarily about Stage 1. The nature of later stages will be indicated towards the end of the presentation. The presentation needs to begin with some general and theoretical background.

Structure of presentation

1. Introduction
2. Background theory
   - (a) Barrier and field definitions
   - (b) "Ideal" FE devices/systems and the orthodoxy test
   - (c) The historical "phases" of FE theory
   - (d) The principal FE special mathematical function v(*x*)
   - (e) FE equation formats
3. Improved analysis of Fowler-Nordheim plots
4. Analysis of Murphy-Good plots
5. Entrenched faults in technological FE literature
6. The empirical FE equation and power-*k* plots
7. Discussion

2a: Barrier and field definitions

The Schottky effect and Schottky constant

Consider a classical surface energy barrier of zero-field height H .

Applying a surface field F_L reduces the classical barrier by an energy Δ_S .

This is the Schottky effect.

Δ_S is given by

$$\Delta_S \equiv c_S F_L^{1/2} .$$

This is the definition of the Schottky constant c_S (or "c") .

It is readily shown that (in the modern International System of Quantities, which uses ε_0 in Coulomb's Law), c_S is given by

$$c_S \equiv (e^3/4\pi\varepsilon_0)^{1/2} ,$$

where e is the elementary positive charge, and ε_0 the vacuum electric permittivity. In FE customary units

$$c_S \cong 1.199\,985 \text{ eV (V/nm)}^{-1/2} \cong 3.794\,868\times10^{-5} \text{ eV (V/m)}^{-1/2} .$$

Two special barrier forms

With models that assume smooth planar metal-like surfaces, two barrier forms are commonly used to model electron potential-energy variation normal to the surface:

the exactly triangular (ET) barrier

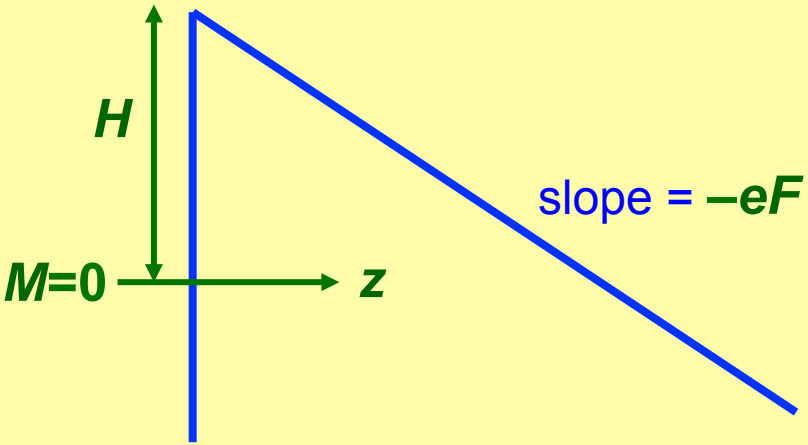

$M(z) = H - eFz$

used by **Fowler & Nordheim (1928)**

the Schottky-Nordheim (SN) barrier

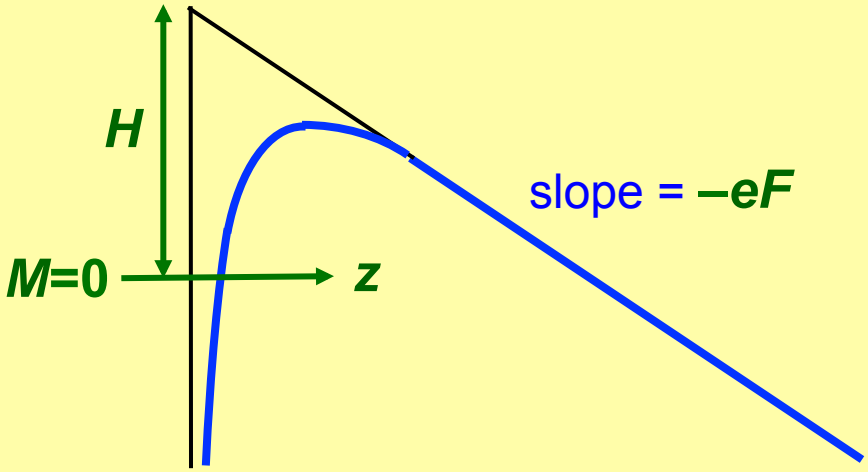

$M(z) = H - eFz - e^2/16\pi\varepsilon_0 z$

used by **Murphy & Good (1956)**

Local barrier fields and scaled fields

At any location "L" on an emitter surface, the local surface field that defines the tunnelling barrier is termed the local barrier field and denoted by F.

A related quantity, the scaled field f [for a barrier of zero-field height ϕ] is formally defined by

$$f \equiv c_S^2 \phi^{-2} F = (e^3/4\pi\varepsilon_0)\phi^{-2}F \cong (1.439\ 965\ \text{eV}^2\ \text{V}^{-1}\ \text{nm})\cdot\phi^{-2}F \ ,$$

where ϕ is the local work function.

This parameter f plays an important role in modern FE theory.

The value f=1 corresponds to the situation where the top of a SN barrier of zero-field height ϕ has been pulled down to the Fermi level. This occurs for a reference field F_R given by

$$F_R \equiv c_S^{-2}\phi^2 \cong (0.694\ 4615\ \text{eV}^{-2}\ \text{V nm}^{-1})\cdot\phi^2 \ .$$

For example, for ϕ = 4.50 eV, $F_R \cong$ 14.1 V/nm.

Advantages of using scaled fields

Advantages of using scaled fields are:

- ✓ can be measured with a FN plot, more accurately than fields;
- ✓ useful for discussing emitter current-voltage behaviour;
- ✓ unifying approach for the different conventions for describing fields;
- ✓ for ideal emitters, are also scaled voltages and macroscopic fields;
- ✓ *f*-ranges are more uniform as between materials than field-ranges;
- ✓ proportional to barrier field, so easy to convert back (multiply by F_R) ;
- ✓ can be used to characterize onset of effects, e.g. turn-on or melting;
- ✓ hence are used in the orthodoxy test.

Advantages of using scaled fields

For example, criteria of emitter behaviour were noted long ago by Dyke and Dolan [R2]**, for one of their experimental systems. These criteria can be expressed in terms of characteristic ("emitter-apex") values (f_C) of scaled field, as shown in the table below (modified from** [R3]**).**

[These f_C -values apply to room-temperature emission, in traditional single-pointed-emitter experimental geometry, for a tungsten emitter (with assumed work function 4.50 eV). For simplicity, J_{kC}^{SN} is calculated using (0 K) SN-barrier theory.]

Criterion	f_C	J_{kC}^{SN} (A/m^2)
Emission onset	0.20	~ 8.7×10^{4}
Safe steady-current limit	0.34	~ 2.3×10^{9}
Onset of space-charge effects	0.49	~ 2.3×10^{11}
Safe pulsed-current limit	0.60	~ 1.7×10^{12}
Breakdown of (0 K) MG theory	~ 0.8	~ 1.6×10^{13}
Apex barrier pulled down to Fermi level.	1.00	–

2b: Ideal FE devices/systems and the orthodoxy test

Ideal devices/systems

At any location "L" on the emitter surface, the field F can be related to the measured voltage V_m by

$$F = V_m/\zeta_L ,$$

where ζ_L is the local voltage conversion length (VCL). ζ_L is a characterization parameter, not a physical length.

A FE device/system is ideal if

(a) at every emitter location "L", ζ_L is effectively constant (with a location-dependent value); and

(b) the measured current I_m is equal to the emission current I_e .

Slope-related characterization parameters

Measured current-voltage $I_m(V_m)$ data taken from an ideal FE device/system can be used to make an "ideal" Fowler-Nordheim (FN) plot of type $\ln\{I_m/V_m^2\}$ vs $1/V_m$.

From the slope S^{fit} of a straight line fitted to this ideal $I_m(V_m)$-type FN plot, an "ideal" characteristic VCL-value can be extracted using

$$\zeta_C^{ideal} = \zeta_C^{extr} = -S^{fit}/s_t b\phi^{3/2} ,$$

where b [$\cong 6.830890\ eV^{-3/2}\ V\ nm^{-1}$] is the second FN constant, and s_t is the fitting value of the slope correction function s (see [R4]).

Slope-related characterization parameters

Measured current-voltage $I_m(V_m)$ data taken from an ideal FE device/system can be used to make an "ideal" Fowler-Nordheim (FN) plot of type $\ln\{I_m/V_m^2\}$ vs $1/V_m$.

From the slope S^{fit} of a straight line fitted to this ideal $I_m(V_m)$-type FN plot, an "ideal" characteristic VCL-value can be extracted using

$$\zeta_C^{ideal} = \zeta_C^{extr} = -S^{fit}/s_t b\phi^{3/2} ,$$

where b [$\cong 6.830890\ eV^{-3/2}\ V\ nm^{-1}$] is the second FN constant, and s_t is the fitting value of the slope correction function s (see [R4]).

If wanted, an "ideal" characteristic field enhancement factor (FEF) γ_{MC}^{ideal} can be found using

$$\gamma_{MC}^{ideal} = d_M/\zeta_C^{ideal} ,$$

where is d_M the relevant system macroscopic distance.

Non-ideal devices/systems

A non-ideal FE device/system has leakage current and/or ξ_L not constant.

The related non-ideal FN plots are likely to be defective, and may yield spurious results for characterization parameters.

Recognised causes of non-ideality include (amongst others):

- current-dependence in field enhancement factors;
- series resistance in the measurement circuit;
- field-dependent geometry (e.g., due to Maxwell-stress effects);
- heating-dependent changes in work function (due to adsorbate removal);
- effects due to field emitted vacuum space charge.

Non-ideal devices/systems

A non-ideal FE device/system has leakage current and/or ξ_L not constant.

The related non-ideal FN plots are likely to be defective, and may yield spurious results for characterization parameters.

Recognised causes of non-ideality include (amongst others):

- current-dependence in field enhancement factors;
- series resistance in the measurement circuit;
- field-dependent geometry (e.g., due to Maxwell-stress effects);
- heating-dependent changes in work function (due to adsorbate removal);
- effects due to field emitted vacuum space charge.

This presentation is about ideal devices/systems, which need to be considered first.

There exists an orthodoxy test [R5] that can be applied to an experimental FN plot to determine whether the results are ideal.

2c: The historical phases of FE theory

Basics of field electron emission equations

The core form of a FE equation gives the local emission current density (LECD) J_L in terms of local work function ϕ and local barrier field F.

The emission current I_e is found by integrating over the emitter surface and writing the result as

$$I_e = \int J_L \, dA \equiv A_{nC} J_C ,$$

where J_C is the characteristic LECD at some chosen characteristic location "C" (often the emitter apex), and A_{nC} is the related notional emission area.

For ideal emitters $I_m = I_e$, so we can write

$$I_m = A_{nC} J_C .$$

The different "historical phases" of FE theory use different expressions for $J_L(\phi,F_L)$, and hence for $J_C(\phi,F_C)$, where F_C is the characteristic barrier field at location "C".

The Fowler-Nordheim historical phase

1. The Fowler-Nordheim phase is based on the original (1928) FN equation [R6, as corrected in R7; see R8 for a modern re-derivation]**:**

$$J_C^{orig} = P_F^{FN} a\phi^{-1} F_C^2 \exp[-b\phi^{3/2}/F_C] ,$$

where *a* and *b* are the FN constants [R8]**, and P_F^{FN} is a field-independent transmission pre-factor [details are unimportant]. This equation is derived using an exactly triangular (ET) tunnelling barrier.**

The so-called elementary FE equation omits the pre-factor, yielding

$$J_C^{el} = a\phi^{-1} F_C^2 \exp[-b\phi^{3/2}/F_C] .$$

The Murphy-Good historical phase

2. The Murphy-Good (MG) phase assumes tunnelling through a planar image-rounded barrier, often now called a Schottky-Nordheim (SN) barrier.. The zero-temperature version of the MG (1956) FE equation ([R9], see [R4] for a modern re-derivation) **can be written in the linked form**

$$J_C^{MG0} = t_F^{-2} J_{kC}^{SN} ,$$

$$J_{kC}^{SN} \equiv a\phi^{-1} F_C^{\,2} \exp[-b v_F \phi^{3/2}/F_C] .$$

with J_{kC}^{SN} the (characteristic) kernel current density for the SN barrier.

v_F and t_F are particular values of the FE special mathematical functions $v(x)$ and $t_1(x)$ where x is the Gauss variable (i.e., the independent variable in the Gauss Hypergeometric Differential Equation). These functions are discussed below. v_F and t_F are found by setting $x=f_C$, e.g. $v_F = v(x=f_C)$, where f_C is the characteristic scaled field corresponding to barrier field F_C.

The Murphy-Good historical phase

2. The Murphy-Good (MG) phase assumes tunnelling through a planar image-rounded barrier, often now called a Schottky-Nordheim (SN) barrier.. The zero-temperature version of the MG (1956) FE equation ([R9], see [R4] for a modern re-derivation) **can be written in the linked form**

$$J_C^{MG0} = t_F^{-2} J_{kC}^{SN} ,$$

$$J_{kC}^{SN} \equiv a\phi^{-1} F_C^{2} \exp[-b v_F \phi^{3/2}/F_C] .$$

with J_{kC}^{SN} the (characteristic) kernel current density for the SN barrier.

v_F and t_F are particular values of the FE special mathematical functions $v(x)$ and $t_1(x)$ where x is the Gauss variable (i.e., the independent variable in the Gauss Hypergeometric Differential Equation). These functions are discussed below. v_F and t_F are found by setting $x=f_C$, e.g. $v_F= v(x=f_C)$, where f_C is the characteristic scaled field corresponding to barrier field F_C.

In the MG (1956) paper, formal expressions for v_F and t_F were given in terms of complete elliptic integrals; subsequently, many (about 20) different approximations for v_F were developed.

[This approach in terms of x and f replaces an older approach in terms of the Nordheim parameter $y=f^{1/2}$, which is now considered less satisfactory.]

21st Century SPME theory

3. 21st century smooth-planar-metal-like-emitter (SPME) theory includes two post-2000 developments.

(a) Better understanding of the mathematics of $v(x)$ including an exact series expansion, and a simple good approximation. [This new understanding in fact subtlely changes the physics.]

(b) Replacing the factor t_F^{-2} by a more general pre-exponential correction factor λ_C that serves as a knowledge uncertainty factor. This leads to the so-called Extended Murphy-Good (EMG) FE equation for LECD:

$$J_C^{EMG} = \lambda_C J_{kC}^{SN},$$

with J_{kC}^{SN} as before. My current thinking (see [R10]) **is that λ_C probably lies in the range $0.005<\lambda_C<14$.**

21st Century SPME theory

3. 21st century smooth-planar-metal emitter (SPME) theory includes two post-2000 developments.

(a) Better understanding of the mathematics of v(x) including an exact series expansion, and a simple good approximation. [This new understanding in fact subtlely changes the physics.]

(b) Replacing the factor t_F^{-2} by a more general pre-exponential correction factor λ_C that serves as a knowledge uncertainty factor. This leads to the so-called Extended Murphy-Good (EMG) FE equation for LECD:

$$J_C^{EMG} = \lambda_C J_{kC}^{SN},$$

with J_{kC}^{SN} as before. My current thinking (see [R8]) is that λ_C probably lies in the range $0.005<\lambda_C<14$.

For an ideal emitter, the EMG equation for measured current I_m^{EMG} is

$$I_m^{EMG} = A_f^{SN} J_{kC}^{SN}$$

where the formal emission area for the SN barrier A_f^{SN} is given by

$$A_f^{SN} = \lambda_C A_{nC} .$$

The merit of the EMG equation for current

As just indicated, for an ideal emitter, the EMG equation for measured current I_m^{EMG} is

$$I_m^{EMG} = A_f^{SN} J_{kC}^{SN}.$$

The merit of this equation is as follows.

For given values of local work function and characteristic local barrier field, the kernel current density J_{kC}^{SN} can be calculated ***exactly***.

The current I_m^{EMG} can be measured ***precisely***.

Hence the formal emission area A_f^{SN} (assuming a SN barrier) is, in principle, ***well-defined***.

Hence, the overall scientific problem can be split into two parts.

(1) The theory of how to measure A_f^{SN} precisely.

(2) The theory of how to interpret measured A_f^{SN}–values in terms of FE theory and the geometrical properties of the emitter.

My interests are currently in the first of these problems, because it needs to be solved before substantial further scientific progress can be made.

2d: The principal FE special mathematical function v(*x*)

The FE special mathematical function v(*x*)

My general strategy for dealing with "v_F" has been:

(a) Make a distinction between "modelling aspects" and "purely mathematical aspects".

Distinguish between the barrier-form correction factor ν_F^{SN} ("nu") used in modelling the SN barrier, and the mathematical function v_F ("vee").

(b) In the mathematics, use the Gauss variable *x* rather than the Nordheim parameter *y* [$=+x^{1/2}$] . Thus write: v(*x*).

(c) When discussing current-voltage characteristics and FN plots, use barrier fields and scaled fields *f* , noting $v_F = v(x=f)$.

(d) When integrating over energies, the Nordheim parameter *y* is often useful, but I prefer to see this as an alternative modelling parameter, given by $y=+f^{1/2}$.

(e) In general terms, build a mathematical theory of v(*x*) that is analogous to the mathematical theory of sin(*x*) as developed 200 or so years ago.

The exact series expansion for v(*x*)

We now know an exact series expansion for v(*x*) [R11, but replace the symbol ***I'*** used there by the symbol ***x*** now preferred]**. The lowest few terms are:**

$$\mathrm{v}(x) = 1 - \left(\frac{9}{8}\ln 2 + \frac{3}{16}\right)x - \left(\frac{27}{256}\ln 2 - \frac{51}{1024}\right)x^2 - \left(\frac{315}{8192}\ln 2 - \frac{177}{8192}\right)x^3 - \ldots$$
$$+ \left(\frac{3}{16} + \frac{9}{512}x + \frac{105}{16384}x^2 + \ldots\right) x\ln x$$

It is also possible to write this in the form

$$\mathrm{v}(x) = (1-x)\cdot[1 + P_\infty(x)] + x\ln x \cdot Q_\infty(x)$$

where $P_\infty(x)$ and $Q_\infty(x)$ are two different infinite power series in *x* .

Note that no terms in $x^{1/2}$ appear in this exact series expansion. This shows that *x* (rather than *y* [= $x^{1/2}$]) is the natural mathematical variable to use for the argument of v.

High-precision formulae for v(*x*) and u(*x*)

High-precision (HP) formulae for v(*x*) and u(*x*) (accurate to better than 8×10^{-10} in $0\le x\le1$) exist, and have been implemented on a spreadsheet:

$$v(x) \cong (1-x)\left(1+\sum_{i=1}^{4} p_i x^i\right) + x\ln x \sum_{i=1}^{4} q_i x^{i-1}$$

$$u(x) \cong u_1 - (1-x)\sum_{i=0}^{5} s_i x^i - \ln x \sum_{i=0}^{4} t_i x^i$$

i	p_i	q_i	s_i	t_i
0	-	-	0.053 249 972 7	0.187 5
1	0.032 705 304 46	0.187 499 344 1	0.024 222 259 59	0.035 155 558 74
2	0.009 157 798 739	0.017 506 369 47	0.015 122 059 58	0.019 127 526 80
3	0.002 644 272 807	0.005 527 069 444	0.007 550 739 834	0.011 522 840 09
4	0.000 089 871 738 11	0.001 023 904 180	0.000 639 172 865 9	0.003 624 569 427
5	-	-	–0.000 048 819 745 89	-
$u_1 = 3\pi/8\sqrt{2} \cong 0.8330405509$				

The numerical expression for v(*x*) can be written formally as:

$$v(x) \cong (1-x)[1 + P_{HP}(x)] + x\ln x \cdot Q_{HP}(x)$$

Simple good approximation for v(*x*)

A "simple good approximation" has also been found for v(*x*)

$$v(x) \approx 1 - x + (x/6)\ln x \,.$$

Over the range $0 \le x \le 1$, v(*x*) has values lying in the range $1 \ge v(x) \ge 0$.

Over this range, the expression above has absolute accuracy of 0.0024 or better, and relative accuracy of 0.33% or better.

This accuracy is sufficient for nearly all room-temperature technological purposes.

The mathematical structure of v(*x*)

Putting these things together, we have:

Exact series expansion:

$$v(x) = (1-x)[1 + P_{\infty}(x)] + x\ln x \cdot Q_{\infty}(x) .$$

High-precision formula:

$$v(x) \cong (1-x)[1 + P_{HP}(x)] + x\ln x \cdot Q_{HP}(x) .$$

Simple good approximation:

$$v(x) \approx (1- x) + x\ln x \cdot (1/6) .$$

All of these expressions have the same basic form: an expression that multiplies (1–*x*) PLUS an expression that multiplies *xlnx*.

The function v(*x*) is mathematically unusual, because its precise definition as a series expansion requires TWO infinite power series.

Special mathematical functions related to v(*x*)

Other FE special mathematical functions (SMFs) are defined as below.
In SN barrier theory they have roles as shown (when $x \rightarrow f$).

$u(x)$	$\equiv -dv/dx$	[$u(f)$ is $-dv/df$]
$t_1(x)$	$\equiv v - (4/3)\, x\, dv/dx$	[$t_1(f)$ is 1st-order Taylor correction factor]
$t_2(x)$	$\equiv v/(1-x)$	[$t_2(f)$ is 2nd-order Taylor correction factor]
$s(x)$	$\equiv v - x\, dv/dx$	[$s(f)$ is slope correction factor]
$w(x)$	$\equiv ds/d(1/x)$	[$w(f)$ is curvature correction factor]
$r(x)$	$\equiv \exp(\eta\, u)$	[$r(f)$ is 2012 intercept correction factor]

Here η [$\cong 9.836\,239\ (eV/\phi)^{1/2}$] is a scaling parameter defined below.
In the literature, $t_1(f)$ is often simply denoted by "t" or "t_F".

2e: Equation formats in Murphy-Good FE theory

Equation formats

The kernel current density for the SN barrier can be written in many different formats.

The following slides illustrate the most useful formats.

The primary scaled format for J_k^{SN}

As already encountered, in conventional barrier-field format the kernel current density for the SN barrier is:

$$J_k^{SN} = a\phi^{-1}F^2 \exp[-v_F b\phi^{3/2}/F] .$$

Substitute $F=f F_R$, and define ϕ-dependent parameters $\eta(\phi)$ and $\theta(\phi)$ by

$$\eta(\phi) = b\phi^{3/2}/F_R = bc_S^2\phi^{-1/2} ,$$

$$\theta(\phi) = a\phi^{-1}F_R^2 = ac_S^{-4}\phi^3 ,$$

where bc_S^2 [≈ 9.836239 $eV^{1/2}$] and ac_S^{-4} [≈ 7.433979×10^{11} A m^{-2} eV^{-3}] are universal constants.

In scaled format (more precisely, "exact *f*-based one-term scaled format") the expression for J_k^{SN} becomes

$$\boxed{J_k^{SN} = \theta f^2 \exp[-\eta\, v(f)/f] .}$$

For example, for ϕ= 4.50 eV, then η≈ 4.64, $\theta \approx 6.77\times10^{13}$ A/m^2.

This form is useful because there is only one independent variable (*f*).

Exact 2-term scaled format for J_k^{SN}

As just seen, the scaled-format expression for J_k^{SN} is

$$J_k^{SN} = \theta f^2 \exp[-\eta\, v/f] \; .$$

From earlier, with $x \rightarrow f$, $v = s - uf$, and $r \equiv \exp[\eta\, u]$. Hence:

$$J_k^{SN} = \theta f^2 \exp[\eta\, u] \exp[-s\eta/f] = r\theta f^2 \exp[-s\eta/f] \; .$$

This is the exact (f-based) two-term scaled format for J_k^{SN} (also called "slope format").

["Scaled" means the scaling parameter η is in the formula.]
["Two-term" means the expression used for $v(f)$ has two terms.]

Exact 2-term scaled format for J_k^{SN}

As just seen, the scaled-format expression for J_k^{SN} is

$$J_k^{SN} = \theta f^2 \exp[-\eta\, v/f] \; .$$

From earlier, with $x \rightarrow f$, $v = s - uf$, and $r \equiv \exp[\eta\, u]$. Hence:

$$J_k^{SN} = \theta f^2 \exp[\eta\, u] \exp[-s\eta/f] = r\theta f^2 \exp[-s\eta/f] \; .$$

This is the exact (f-based) two-term scaled format for J_k^{SN} (also called "slope format").

["Scaled" means the scaling parameter η is in the formula.]
["Two-term" means the expression used for $v(f)$ has two terms.]

This formula can ALSO be derived from the first two terms of a Taylor expansion of $v(f)$ about an arbitrary value f_t .

Many approximate expressions exist for $v(f)$, so many approximate expressions/values exist for $r(f)$ and $s(f)$. High-precision expressions also exist.

Good 3-term scaled format for J_k^{SN}

As just seen, the scaled-format expression for J_k^{SN} is

$$J_k^{SN} = \theta f^2 \exp[-\eta v/f] .$$

The "simple good approximation" $v=1-f+(f/6)\ln f$, can be used to derive the good (f-based) three-term scaled format

$$J_k^{SN} \approx \theta \exp\eta \; f^{(2-\eta/6)} \exp[-\eta/f] .$$

Local-field-based scaled formats

In all cases it is true that:

$$\eta / f = b\phi^{3/2}/F \; ; \quad \theta f^2 = a\phi^{-1}F^2 \; .$$

These expressions can be substituted into any of the *f*-based scaled formats.

For example, the good *f*-based three-term scaled format

$$J_k^{SN} \approx \theta \exp\eta \; f^{(2-\eta/6)} \exp[-\eta / f \,]$$

becomes

$$J_k^{SN} \approx a\phi^{-1} \cdot \exp\eta \cdot F^{(2-\eta/6)} \cdot \exp[-b\phi^{3/2}/F \,] \; .$$

Measured-voltage-based scaled formats

For ideal FE devices/systems, it is true that:

$$f = V_m/V_{mR},$$

where V_{mR} is the reference measured voltage for which f=1 and the top of a SN barrier (of zero-field height ϕ) is pulled down to the Fermi level.

This expression can be substituted into any of the f-based scaled formats.

For example, the good f-based three-term scaled format

$$J_k^{SN} \approx \theta \exp\eta \; f^{(2-\eta/6)} \; \exp[-\eta/f]$$

becomes

$$J_k^{SN} \approx \theta \exp\eta \; (V_m/V_{mR})^{(2-\eta/6)} \exp[-\eta \, V_{mR}/V_m] .$$

Measured-voltage-based scaled formats

For ideal FE devices/systems, it is true that:

$$f = V_m/V_{mR},$$

where V_{mR} is the reference measured voltage for which f=1 and the top of a SN barrier (of zero-field height ϕ) is pulled down to the Fermi level.

This expression can be substituted into any of the f-based scaled formats.

For example, the good f-based three-term scaled format

$$J_k^{SN} \approx \theta \exp\eta \; f^{(2-\eta/6)} \; \exp[-\eta/f]$$

becomes

$$J_k^{SN} \approx \theta \exp\eta \; (V_m/V_{mR})^{(2-\eta/6)} \exp[-\eta \, V_{mR}/V_m] .$$

And the Extended Murphy-Good (EMG) FE equation for $I_m(V_m)$ can be written in voltage-based scaled format as

$$I_m^{EMG} = A_f^{SN} J_k^{SN} \approx A_f^{SN} \theta \exp\eta \; (V_m/V_{mR})^{(2-\eta/6)} \exp[-\eta \, V_{mR}/V_m] .$$

where V_{mR} here is the reference measured voltage for the characteristic location "C". We return to this equation in connection with Murphy-Good plots

3. Analysis of *ideal* FN plots

Slope-related characterization parameters

As already indicated, from the slope S^{fit} of a straight line fitted to an ideal $I_m(V_m)$-type FN plot, a characteristic VCL can be extracted using

$$\zeta_C^{extr} = -S^{fit}/s_t b\phi^{3/2} ,$$

where s_t is the fitting value of the slope correction function s .

If wanted, a characteristic field enhancement factor (FEF) γ_{MC}^{extr} can be found from

$$\gamma_{MC}^{extr} = d_M/\zeta_C^{extr} ,$$

where is d_M the relevant system macroscopic distance.

The intercept fitting value r_t

Fitting values of s(*f*) and r(*f*) are defined by s_t=s(f_t), r_t=r(f_t), where the fitting value f_t relates to the measured-voltage value where the experimental FN plot is parallel to the tangent to the theoretical FN plot.

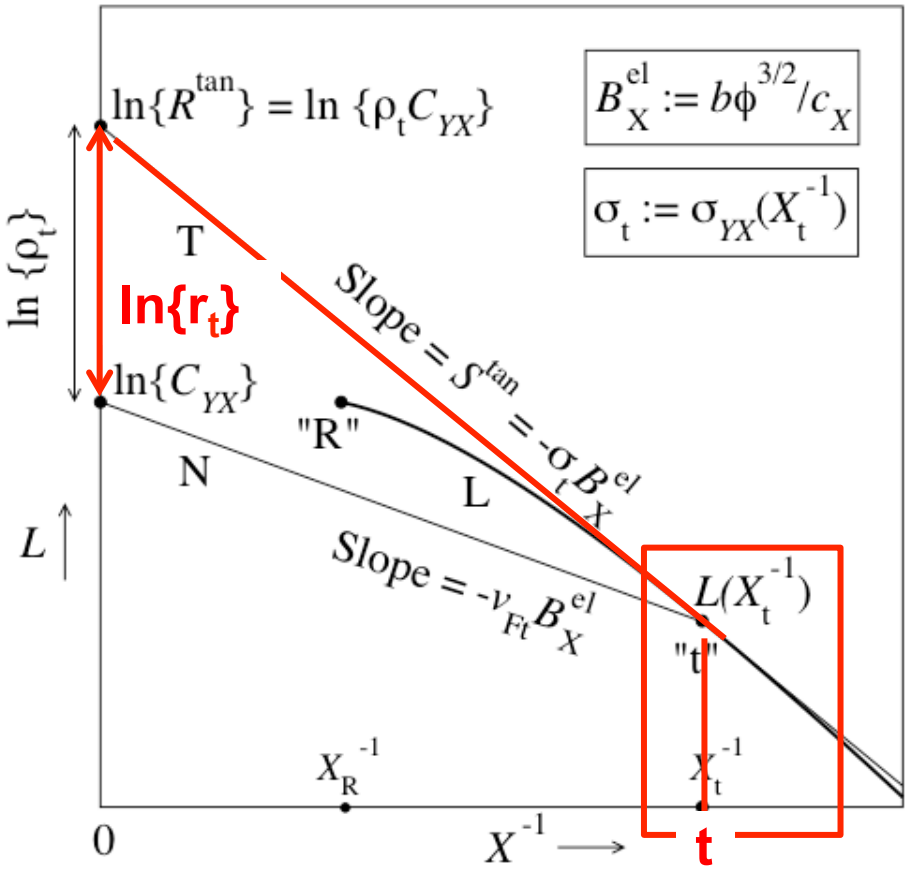

This a general diagram that applies to many barriers and equations

For the EMG FE equation:

$$C_{YX} = A_f^{SN}\, a\phi^{-1} F_C^{\,2}\,.$$

For the SN barrier

$$\rho_t = r_t\,.$$

Also (in scaled format): $X_t = f_t$.

The value of r_t depends on the choice of "fitting point" "t" .

The intercept fitting value r_t

Fitting values of s(*f*) and r(*f*) are defined by s_t=s(f_t), r_t=r(f_t), where the fitting value f_t relates to the measured-voltage value where the experimental FN plot is parallel to the tangent to the theoretical FN plot.

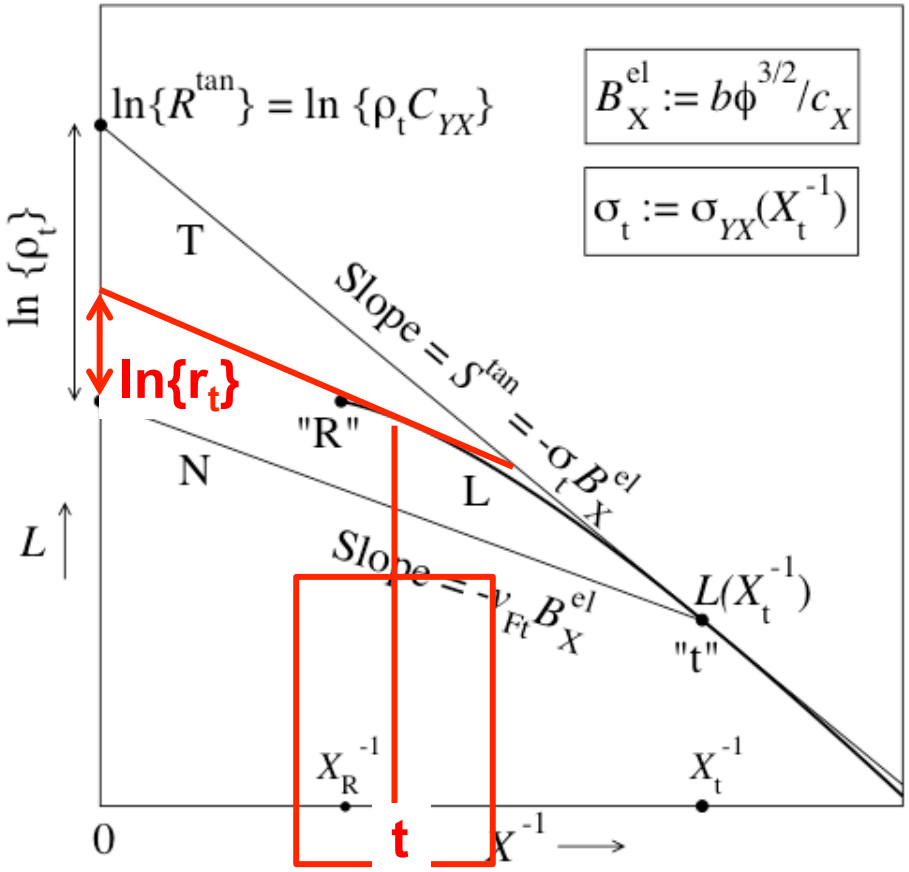

This a general diagram that applies to many barriers and equations

For the EMG FE equation:

$$C_{YX} = A_f^{SN}\, a\phi^{-1} F_C^{\,2}\,.$$

For the SN barrier

$$\rho_t = r_t\,.$$

Also (in scaled format): $X_t = f_t$.

The value of r_t depends on the choice of "fitting point" "t" .

Area extraction using an extraction parameter

Let $\ln\{R_{FN}^{fit}\}$ be the intercept of a line fitted to an ideal $I_m(V_m)$ FN plot.

In the tangent method, as applied using the Extended Murphy-Good (EMG) FE equation, we have:

from: slope: $$S_{FN}^{fit} = -s_t\, b\phi^{3/2}\zeta_C \;;$$

from: intercept: $$R_{FN}^{fit} = r_t\, A_f^{SN} a\phi^{-1}\zeta_C^{-2} \;.$$

Hence: $$R_{FN}^{fit}\,(S_{FN}^{fit})^2 = (ab^2)\,(r_t s_t^2)\,\phi^2\,A_f^{SN} \;.$$

This has eliminated ζ_C and we can write

$$\boxed{A_f^{SN} \equiv \Lambda^{SN}(\phi, f_t)\;[R_{FN}^{fit}\,(S_{FN}^{fit})^2]\;,}$$

where (for a FN plot) the extraction parameter for the SN barrier $\Lambda_{FN}^{SN}(\phi, f_t)$ is defined as above and given by

$$\boxed{\Lambda_{FN}^{SN}(\phi, f_t) = 1/[(ab^2\phi^2)\,(r_t s_t^2)]\;.}$$

The value of $ab^2 \cong 7.192492 \times 10^{-5}$ A eV^{-2} nm^2 .

Formal area efficiency for a LAFE

Large-area field electron emitters (LAFEs), such as carbon nanotube arrays, contain very many individual emitters. For a LAFE, the formal emission area A_f^{SN} derived from an $I_m(V_m)$-type FN plot is always very much less than the LAFE macroscopic (or "footprint") area A_M. The formal area efficiency α_f^{SN}, defined by

$$\alpha_f^{SN} \equiv A_f^{SN} / A_M ,$$

is a measure of what fraction of the LAFE is actually emitting electrons. Obviously, the area efficiency α_f^{SN} can be derived from an ideal LAFE $I_m(V_m)$-type FN plot if A_M is known.

$J_M(F_M^{app})$ plots for a LAFE

For a LAFE, the (measured) macroscopic (or "LAFE-average") current density J_M is defined by

$$J_M \equiv I_m / A_M ,$$

and a parameter F_M^{app} called here an apparent macroscopic field can be defined by

$$F_M^{app} \equiv V_m / d_M ,$$

where, as before, d_M is the relevant system macroscopic distance. [For the common parallel-planar-plate geometry, d_M is the separation between the plates; other interpretations are needed in other geometries.]

$J_M(F_M^{app})$ plots for a LAFE

For a LAFE, the (measured) macroscopic (or "LAFE-average") current density J_M is defined by

$$J_M \equiv I_m / A_M ,$$

and a parameter F_M^{app} called here an apparent macroscopic field can be defined by

$$F_M^{app} \equiv V_m / d_M ,$$

where, as before, d_M is the relevant system macroscopic distance. [For the common parallel-planar-plate geometry, d_M is the separation between the plates; other interpretations are needed in other geometries.]

The literature contains many examples of $J_M(F_M^{app})$ FN plots, i.e. plots of the form $\ln\{J_M/(F_M^{app})^2$ vs $1/F_M^{app}$. However, for a non-ideal emitter this methodology is flawed [R12], because the mathematical parameter F_M^{app} as defined by the equation above may not be a true electrostatic field, and extracted characterization-parameter-values may be spurious.

It is strongly recommended that FN plots should always be made using raw measured $I_m(V_m)$ data, and that an orthodoxy test should be applied before further analysis.

Slope and intercept correction factors

From definitions earlier (putting $x \rightarrow f$):

$u(f) \equiv -\,dv/df$

$s(f) \equiv v - f\,dv/df$ [s(*f*) is slope correction factor]

$r(f) \equiv \exp(\eta\, u)$ [r(*f*) is 2012 intercept correction factor]

So, if ϕ is known, and an expression for v(*f*) is assumed, all relevant correction factors can be expressed as functions of *f* .

Extraction parameter comparisons

The fitting value f_t is not initially known. Usual approach is to define a first approximation "f_{t0}" by $s(f_{t0}) = 0.95$. Spreadsheet manipulations, using high-precision (HP) formulae, yield $f_{t0} \approx 0.2815$. Related values are: $r_{t0} \approx 125.05$, $r_{t0}s_{t0}^2 \approx 112.86$.

For $\phi = 4.50$ eV, this yields: $\Lambda_{FN}^{SN} \sim 6.1$ nm^2/A .

The HP result for $r_{t0}s_{t0}^2$ can be compared with results (for $f_t = f_{t0}$) derived from the 1970s approximations most commonly used in FE literature:

who	v	u	s	r	r*s*s	discrepancy
Forbes-Deane	HP	1.041	0.950	125.055	112.862	0%
"Simple good"	1-f+(f/6)lnf	1.045	0.952	126.928	115.079	2%
Charbonnier-Martin	0.956-1.062f	1.062	0.956	137.597	125.755	11%
Spindt et al	0.95-f	1.000	0.950	103.218	93.155	-17%
Elinson-Shrednik	0.95-1.03f	1.030	0.950	118.623	107.058	-5%

Now that the high-precision (HP) formulae are easily available, all of the 1970s (etc.) approximations are OBSOLETE.

Note use of the high-precision (HP) formulae is marginally better than use of the "simple good approximation".

Limitations of FN plots

However, even with the use of high-precision formulae, it remains difficult to extract well-defined characterization parameters from a FN plot.

This is because Murphy-Good FE theory (and more sophisticated FE theories) predict FN plots to be slightly curved.

In MG and EMG theory, if high-precision results are required, this causes difficulties of two kinds when fitting a straight line to a curved FN plot:

(a) The fitting value f_t of scaled field (which is initially unknown) must be determined precisely.

(b) Because the fitted line represents a chord to the theoretical FN plot, rather than the tangent to the plot, a chord correction must be applied.

It emerges that both these corrections depend on the range of f-values that the experimental data relate to. The combined extraction parameter varies accordingly. For ϕ= 4.50 eV, simulations suggest a maximum range for the combined extraction parameter Λ^{comb} of approximately

$$3.3 < \Lambda^{comb} < 9.3 .$$

Limitations of FN plots

A further difficulty is that the relevant range of *f*-values is not initially known.

All this suggests we look for a form of plot that IS theoretically expected to be a straight line (or very nearly a straight line).

The most obvious possibility is the Murphy-Good plot described below.

A Murphy-Good plot is a special form of power-*k* plot. It is convenient to first give the theory of this more general form of data plot.

4. Murphy-Good plots

[see R13]

The power-*k* and Murphy-Good plots

For any value of *k*, the so-called empirical FE equation has the form

$$I_m = C V_m^k \exp[-B/V_m] ,$$

where *k*, *C* and *B* are initially treated as constants. Hence:

$$\ln\{I_m/V_m^k\} = \ln\{C\} - B/V_m ,$$

A plot of $\ln\{I_m/V_m^k\}$ vs $1/V_m$ is termed a power-*k* plot .

If *k*, *C* and *B* are constant, then the plot should be exactly straight.

A Murphy-Good (MG) plot is a special form of power-*k* plot for which

$$k = 2 - \eta/6 .$$

MG plots can be used with both the 1956 MG FE equation and the Extended MG (EMG) FE equation. Theory is given below for the EMG FE equation, since this is more general.

Basic theory of power-*k* plots

The empirical FE equation is

$$I_m = C V_m^k \exp[-B/V_m] .$$

The equivalent equation in terms of characteristic scaled field f_C is

$$I_m = C_f f_C^k \exp[-B_f/f_C] ,$$

where C_f and B_f are constants related to C and B .

Using $f_C = V_m/V_{mR}$ yields

$$I_m = C_f (V_m/V_{mR})^k \exp[-B_f V_{mR}/V_m] .$$

Hence

$$\ln\{I_m/V_m^k\} = \ln\{C_f V_{mR}^{-k}\} - B_f V_{mR}/V_m .$$

Basic theory of power-*k* plots

$$\ln\{I_m/V_m^{\,k}\} = \ln\{C_f V_{mR}^{\,-k}\} - B_f V_{mR}/V_m \,.$$

Hence, for an ideal FE device/system, the slope S^{fit} and intercept $\ln\{R^{fit}\}$ of a straight line fitted to a power-*k* plot are given by

$$S^{fit} = -B_f V_{mR} \,,$$

$$R^{fit} = C_f V_{mR}^{\,-k} \,.$$

Hence:

$$C_f = R^{fit} |S^{fit}|^k / B_f^{\,k} \,.$$

The value of B_f is normally known, so the value of C_f can be determined (without the uncertainties associated with FN plots).

Area extraction parameter for MG plot

From earlier, the Extended Murphy-Good (EMG) FE equation for $I_m(V_m)$, in voltage-based scaled format, is

$$I_m^{EMG} \approx A_f^{SN}\,\theta\,\exp\eta\,(V_m/V_{mR})^{(2-\eta/6)}\exp[-\eta\,V_{mR}/V_m]\,.$$

By comparison with earlier equation

$$I_m = C_f\,(V_m/V_{mR})^k \exp[-B_f\,V_{mR}/V_m]\,,$$

we find:

$$k = 2-\eta/6\,,$$

$$B_f = \eta\,,$$

$$C_f = A_f^{SN}\,\theta\,\exp\eta\,.$$

From previous slide: $C_f = R^{fit}\,|S^{fit}|^k / B_f^{\,k}$.

Hence:

$$\{A_f^{SN}\}^{extr} = \Lambda_{MG}(\phi)\,R^{fit}\,|S^{fit}|^{(2-\eta/6)}\,,$$

where the area extraction parameter for the MG plot, $\Lambda_{MG}(\phi)$, is given by

$$\Lambda_{MG}(\phi) = 1/[\theta\,\exp\eta\cdot\eta^{(2-\eta/6)}]\,.$$

From definitions given earlier, $\theta\eta^2 = ab^2\phi^2$, hence

$$\Lambda_{MG}(\phi) = 1/[(ab^2\phi^2)(\exp\eta\;\eta^{-\eta/6})]\,.$$

Comparison of extraction-parameter formulae

For the **Murphy-Good (MG) plot**, the area extraction parameter is given by

$$\Lambda_{MG}(\phi) = 1/[(ab^2\phi^2)(\exp\eta\ \eta^{-\eta/6})] .$$

For the **Fowler-Nordheim (FN) plot**, it was shown that the area extraction parameter for the SN barrier is given by

$$\Lambda_{FN}^{SN}(\phi, f_t) = 1/[(ab^2\phi^2)(r_t s_t^2)] .$$

For extracting precise formal-area values, the MG plot is superior to the FN plot because the MG-plot extraction parameter does not need a fitting point to be determined.

Another advantage of a MG plot is that the extraction parameter $\Lambda_{MG}(\phi)$ depends only weakly on work function ϕ, as illustrated in the Table below:

Typical values of $\Lambda_{MG}(\phi)$ and related parameters.

ϕ (eV)	η	$\exp\eta\cdot\eta^{-\eta/6}$	$\Lambda_{MG}(\phi)$ (nm^2/A)
3.50	5.2577	44.85	25.31
4.00	4.9181	37.06	23.45
4.50	4.6368	31.54	21.77
5.00	4.3989	27.46	20.25
5.50	4.1942	24.34	18.89

Parameters related to MG-plot slope

From earlier: $\ln\{I_m/V_m^k\} = \ln\{C_f V_{mR}^{-k}\} - B_f V_{mR}/V_m$.

For an ideal FE device/system, the slope S^{fit} of a straight line fitted to a voltage-based power-k plot or Murphy-Good plot is given by

$$S^{fit} = -B_f V_{mR} = -\eta V_{mR} = -\eta F_R \zeta_C = -b\phi^{3/2}\zeta_C .$$

Hence (1): the characteristic voltage conversion length (VCL) ζ_C^{extr} can be extracted via

$$\zeta_C^{extr} = -S^{fit}/b\phi^{3/2} .$$

A minor advantage of this formula is that it does NOT contain the slope correction factor that appears in FN-plot theory.

Hence (2): the characteristic barrier-field value F_C^{extr} corresponding to a given measured-voltage (V_m) can be measured using the formula

$$F_C^{extr} = V_m/\zeta_C^{extr} .$$

Hence (3) ...

Parameters related to MG-plot slope

Hence (3): the characteristic-scaled-field value (f_C-value) corresponding a given measured-voltage can be extracted via

$$f_C^{extr} = V_m/V_{mR} = -(\eta/S^{fit})\cdot V_m \,.$$

Extracted f_C-values that define the f-range apparently used in experiments can be used in an orthodoxy test based on an MG plot or power-k plot [R14].

The mathematical consistency of MG plot analysis has been validated by means of simulations.

Interim summary

To improve the interpretation of measured FE current-voltage data, "21st century smooth-planar-metal-like emitter (SPME) theory" has been developed and described.

An immediate task is to persuade FE experimentalists to move to using "21st century SPME theory", when presenting theory or interpreting measured FE current-voltage data.

However, there are a number of entrenched faults in existing literature, and some poor practice, and these issues need to be addressed. These are described next.

5. Entrenched faults in technological FE literature

Entrenched faults (1)

Major faults in technological FE literature include the following.

1. **Use of the original 1928/29 FN FE equation, rather than some form of the MG FE equation** [R15]**.**

   As compared with the MG FE equation, the 1928/29 FN FE equation underpredicts local emission current densities by a factor typically of order 300.

2. **With LAFEs, failure to distinguish between local emission current density and macroscopic current density, and omission (from stated equations in a paper) of a factor relating to area efficiency.**

   This can lead to large discrepancies, whereby the equations given in a paper overpredict (by many orders of magnitude) experimental results shown in data plots.

Entrenched faults (2)

3. **Extraction of characterization parameters from data plots taken from emitters with non-orthodox behaviour. This is a particular problem when raw $I_m(V_m)$ data is pre-converted to $J_M(F_M^{app})$ data before making a FN plot** [R10]**.**

   Extracted values of the characterization parameter "field enhancement factor" can be spuriously high, by a factor of more than 100 in the worst cases.

Occasional minor problems include the following.

4. **Failure to write equations in the dimensionally consistent form required by the 1970s reforms to the international system of measurement.**

   Apart from being "incorrect modern practice", this can lead to minor confusion about the units being used to measure field within the framework of the modern "International System of Quantities (ISQ)".

Entrenched faults (3)

5. **Use of 1960s-style Gaussian-system equations (in which fields would be measured in the SI unit "$J^{1/2}\,m^{-3/2}$", rather than use of the modern "International System of Quantities (ISQ)", in which the SI unit for electrostatic field is "V/m".**

   Apart from being "incorrect modern practice", this can lead to confusion over the meaning of the symbol "*E*" (or "*F*"), and difficulties in evaluating formulae correctly.

Persistent unhelpful practices include:

6. **(In some papers) using the term "Fowler-Nordheim equation" as a name for the equation developed by Murphy and Good in 1956.**

7. **Failure to give references to any recent textbook or to any theoretical paper more recent than the original 1928 FN paper.**

   As noted in [R15]**, these last two things are community practices that appear to contribute to fault #1 noted above.**

Interim summary continued

As stated earlier, the author's belief is that, in order to move FE science forwards, a necessarily *preliminary* step is to take out all the "misconceptions", "outdated/obsolete theory" and "poor practice" in present technological FE literature, and persuade FE experimentalists to move towards consistent use of "21st century SPME methodology", when presenting theory or interpreting measured FE current-voltage data.

Within this methodology, there still are issues of whether multi-parameter numerical fitting would eventually yield more precise results than Murphy-Good plots, and whether multi-parameter numerical fitting (or some other method) could reliably extract an "apparent local work-function value" from measured current-voltage data, particularly when the data is "noisy.

After this preliminary step (called "Stage 1" earlier), one needs to move on to better data analysis procedures, but the necessary theoretical understanding of data-interpretation processes is not yet in place ….

Future Stages of data-analysis theory

Definition: I use the term **point-form emitter** to describe an emitter that is shaped like a pointed needle or a rounded post, or is otherwise "pointy".

With a point-form emitter, in principle there are at least three additional physical effects that need to be taken into account in current-voltage data analysis:

A) The effect of emitter shape on the integration of local emission current density across the emitter surface.

B) The effect of surface shape (in particular, local curvature) on the transmission probability.

C) The effect of atomic structure.

It is also not inconceivable that there could arise fundamental quantum-mechanical difficulties when attempting to make highly accurate calculations of transmission probability effects, for realistically shaped and structured emitters.

Data-analysis theory: Stage 2

Effect (A) on the previous slide can be investigated by using various emitter shapes and the planar transmission approximation. This approximation takes the local emission current density (LECD) at at location "L" to be given by some appropriate version of planar transmission/tunnelling theory, taking the barrier field to be the local barrier field at location "L".

Section 6. summarizes some preliminary investigations into this effect, previously briefly reported in [R16].

6. The empirical FE equation and power-*k* plots

Determining the value of *k*

In point-form emitter theory, the value of *k* will NOT be given by the Murphy-Good formula $k = 2 - \eta/6$.

We need to develop methods for determining the value of *k* experimentally.

But first these need to be tested by simulations.

Two obvious methods are the least-residual method and the local-gradient method. We next begin to explore the first of these.

The least-residuals methods

In power-*k* coordinates, the empirical FE equation has the form

$$\ln\{I_m/V_m^k\} = \ln\{C\} - B/V_m \ .$$

Given a set of $I_m(V_m)$ data points, and a particular value of *k*, a straight line can be fitted to a power-*k* plot of these points by usual regression methods. The sum of the squared deviations of the data points from the fitted line is termed the residual and denoted by $\Re(k)$.

The variation of $\Re(k)$ with *k* is explored, and the *k*-value that yields the least value of $\Re(k)$ (the "least residual") is determined.

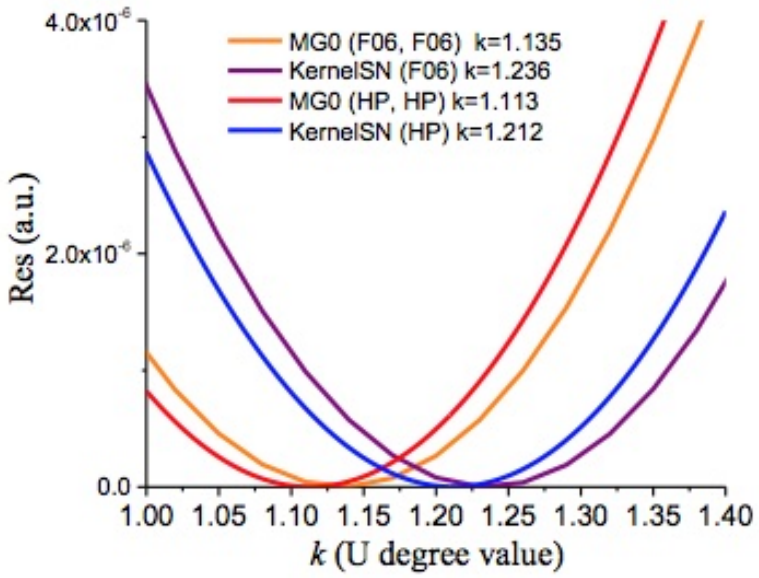

The value of *k* found in this way is relatively well defined, as illustrated in the diagram alongside. [This shows results for four different methods of calculating $I_m(V_m)$ data sets].

Extracted *k*-values for planar-emitter model

Initial tests on the least residual method used the SPME model, and 1970s era planar emission theory, where some results are well known, and the LECD can be written in the slightly generalized form

$$J_L = \tau_F^{-2}\, a\phi^{-1} F_C^{\,2} \exp[-b\nu_F \phi^{3/2}/F_C] \,.$$

Various different approximate forms for J_L, τ_F^{-2} and ν_F are used. [ES= Elinson-Shrednik; F06="simple good approximation"; HP=high precision; MG300=Murphy-Good with 300 K temperature correction factor.]

Test	LECD Equation	τ_F^{-2}	ν_F	Predicted k_t	Derived k_t
1	Elementary	1	1	2.00000	2.00000
2	MG0 (ES, ES)	1/1.1	0.95–1.03*f*	2.00000	2.00000
3	KernelSN (F06)	1	F06	1.23564	1.23560
4	MG0 (F06, F06)	F06	F06	n/a	1.13519
5	KernelSN (HP)	1	HP	n/a	1.21200
6	MG0 (HP, HP)	HP	HP	n/a	1.11320
7	MG300 (F06, F06)	F06	F06	n/a	1.2160

Tests 1 to 3 seem to show that, from good data, *k*-values can be extracted with high accuracy.

The other tests show that the form of pre-exponential has noticeable effects.

Extracted *k*-values for HCP emitter model

Initial tests have also been conducted on a point-form emitter, using the hemisphere-on-cylindrical post (HCP) emitter model, with dimensions compatible with the carbon nanotubes (CNTs) used in experiments at the Ioffe Laboratory in Saint-Petersburg. [SW=single-walled CNTs; MW=multi-walled CNTs.] To investigate the emitter shape effects "in isolation", the planar transmission approximation is used, which neglects the effect of emitter surface curvature on tunnelling probability.

Results for various approximate emission theories are shown on the following slide. Results are given for the least residual (LR) method; some results are also shown for the local gradient (LG) method.

Main conclusions are:

(1) In these simulations, the LR and LG methods give very similar results. [This may not be true for noisy experimental data.]

(2) The difference from the results for the planar emitter model comes from the dependence of emission area on voltage (which contributes to *k*). In all cases tested here, this contribution is about $k_A = 0.5$.

Extracted *k*-values for HCP emitter model

Test	Meth	Type	LECD equation	λ	ν_F	*k* from Table 1	Derived *k*	Change, k_A
8	LR	SW	MG0 (ES)	1/1.1	0.95-1.03*f*	2.00	2.455	+0.455
9	LR	MW	MG0 (ES)	1/1.1	0.95-1.03*f*	2.00	2.463	+0.463
10	LR	SW	KernelSN	1	F06	1.236	1.731	+0.496
11	LR	MW	KernelSN	1	F06	1.236	1.740	+0.504
12	LR	SW	MG0	F06	F06	1.135	1.637	+0.502
13	LR	MW	MG0	F06	F06	1.135	1.646	+0.511
14	LR	SW	KernelSN	1	HP	1.212	1.707	+0.495
15	LR	MW	KernelSN	1	HP	1.212	1.716	+0.504
16	LR	SW	MG0	HP	HP	1.113	1.614	+0.501
17	LR	MW	MG0	HP	HP	1.113	1.624	+0.511
18	LR	SW	MG300	F06	F06	1.216	1.719	+0.503
19	LR	MW	MG300	F06	F06	1.216	1.728	+0.512
20	LG	SW	MG0 (ES)	1/1.1	0.95-1.03*f*	2.00	2.451	+0.451
21	LG	MW	MG0 (ES)	1/1.1	0.95-1.03*f*	2.00	2.464	+0.464
22	LG	SW	MG0	F06	F06	1.135	1.631	+0.496
23	LG	MW	MG0	F06	F06	1.135	1.645	+0.510
24	LG	SW	MG0	HP	HP	1.113	1.611	+0.498
25	LG	MW	MG0	HP	HP	1.113	1.625	+0.510

6. Discussion

Implications for future activity

This work has the following general implications.

1. **There is a need to bring all technological FE up to the level of "21st Century smooth-planar-metal-like-emitter theory".**
2. **As part of this, there is a need to remove the various "pathological" entrenched errors in FE technological literature.**

With the growing attention being paid to issues of research integrity in science, it seems highly desirable to improve the state of FE literature as soon as possible.

3. **It also seems urgent to continue investigations into methods of FE data interpretation that explicitly apply to point-form emitters, by taking emitter shape into account.**
4. **In the longer term, the ability to make accurate comparisons between FE experiment and theory may be of wider interest in tunnelling contexts, in particular in quantum biology.**

References (1)

R1. R.G. Forbes, J.H.B. Deane, A.G. Kolosko, S.V. Fillipov, and E.O. Popov, "Reinvigorating our approach to field emission area extraction (because Murphy-Good plots are better than Fowler-Nordheim plots)", **3**2nd International Vacuum Nanoelectronics Conf. & 12th International Vacuum Electron Sources Conf., Cincinnatti, July 2019. [Technical Digest, p. 23.] doi:10.13140/RG.2.2.32112.81927

R2. W.P. Dyke & J.K. Trolan, "Field emission: large current densities, space charge, nd the vacuum arc", Phys. Rev. **89**, 799–808 (1953).

R3. R.G. Forbes, "Description of field emission current/voltage characteristics in terms of scaled barrier field values (*f*-values)", J. Vac. Sci. Technol. B **26**, 209–213 (2008).

R4. R.G. Forbes & J.H.B. Deane, "Reformulation of the standard theory of Fowler-Nordheim tunneling and cold field electron emission", Proc. R. Soc. Lond. A **463**, 2907–2927 (2007).

R5. R.G. Forbes, "Development of a simple quantitative test for lack of field emission orthodoxy", Proc. R. Soc. Lond. A **469**, 20130271 (2013).

R6. R.H. Fowler & L. Nordheim. "Electron emission in intense electric fields", Proc. R. Soc. Lond. A **119**, 173–181 (1928).

R7. T.E. Stern, B.S. Gossling & R.H. Fowler**,** "Further studies in the emission of electrons from cold metals", Proc. R. Soc. Lond. A **124**, 699–723 (1929).

References (2)

R8. R.G. Forbes & J.H.B. Deane, "Transmission coefficients for the exact triangular barrier: an exact general analytical theory that can replace Fowler & Nordheim's 1928 theory", Proc. R. Soc. Lond. A **467**, 2927–2947 (2011). See Electronic Supplementary Materials for information about universal constants used in field emission.

R9. E.L. Murphy & R.H. Good, "Thermionic emission, field emission and the transition region", Phys. Rev. **102**, 1464–1472 (1956).

R10. R.G. Forbes, "Comparison of the Lepetit field emission current-density calculations with the Modinos-Forbes uncertainty limits", 31st International Vacuum Nanoelectronics Conf., Kyoto, July 2018. [Technical Digest, pp. 126–127.] doi:10.13140/RG.2.2.17153.10080

R11. J.H.B. Deane and R.G. Forbes, "The formal derivation of an exact series expansion for the Principal Schottky-Nordheim Barrier Function *v*, using the Gauss hypergeometric differential equation", J. Phys. A: Math. Theor. **41**, 395301 (2008).

R12. R.G. Forbes, "Why converting field emission voltages to macroscopic fields before making a Fowler-Nordheim plot has often led to spurious characterization results", J. Vac. Sci. Technol. **B 37**, 051802 (2019).

R13. R.G. Forbes, "The Murphy-Good plot: a better method of analysing field emission data", R. Soc. Open Sci. **6**, 190912 (2019)**.**

R14. M.M. Allaham, R.G. Forbes, A. Knápek and M.S. Mousa, "Implementation of the orthodoxy test as a validity check on experimental field emission data" J. Electr. Eng. Slovak **71**, 37–42 (2020).

References (3)

R15. R.G. Forbes, "Comments on the continuing widespread and unnecessary use of a defective equation in field emission related literature", J. Appl. Phys. **126**, 210901 (2019).

R16. E.O. Popov, A.G. Kolosko, S.V. Fillipov, and R.G. Forbes, "Emission area extraction for needle-shaped and post-shaped emitters." [Technical Digest, p. 96.] doi:10.13140/RG.2.2.35337.19041R10. R.G. Forbes, "Comparison of the Lepetit field emission current-density calculations with the Modinos-Forbes uncertainty limits", 31st International Vacuum Nanoelectronics Conf., Kyoto, July 2018. [Technical Digest, pp. 126–127.] doi:10.13140/RG.2.2.17153.10080

Thanks for your attention